Chapter 1

The Finite Element Method with Applications to Fluid Mechanics

K.N. Biraki, K.C. Kyriakoudi, A.C. Felias and M.A. Xenos
Department of Mathematics, University of Ioannina,
Ioannina, 45110, Greece
mxenos@uoi.gr *

Contents

*Correspondence email

Abstract: The finite element method (FEM) is a well established approach for the numerical solution of ordinary differential equations (ODEs) and partial differential equations (PDEs). This method is a powerful tool in the study of various problems and has many applications, such as structural and fluid mechanics. In this review chapter, we mainly focus on applying the method to fluid mechanics problems. Initially, we present the FEM along with the basic theorems and examples. We analyse the error estimates for linear problems and the base functions that help distinguish the problem under consideration. We present the numerical solution of the Duffing equation, using the Galerkin FEM.

Additionally, we concentrate on the two–dimensional Stokes problem. We further introduce novel methods, such as the Discontinuous Galerkin (DG) FEM. The notion of adaptive mesh is also discussed. Lastly, we study the two–dimensional Navier–Stokes equations using the Galerkin FEM. These advanced methods provide reliable numerical results in all studied cases. This is achieved with the application of FEM to "test problems", such as the backward facing step. We obtain all the numerical results utilizing the software programs MATLAB and FEniCS.

MSC: 76M10, 65M60, 65N30, 65L60

Basic Principles of Finite Elements

1. Introduction

Nonlinear differential equations govern a plethora of biological, mechanical and physical phenomena. Most PDEs aren't analytically solvable and to obtain a solution numerical methods are utilized. The finite element method (FEM) is a well established approach for the numerical solution of ODEs and PDEs. A large domain divides into smaller discrete cells, called finite elements, being simple polygonal shapes, forming the computational mesh of this domain. The method excels in its accurate representation of complex geometries, the finite elements of which are approximated by polynomials. Nowadays, FEM is arguably one of the most well established and convenient computational techniques. There is a variety of applications in many fields, such as mechanical design, structural analysis, fluid flow, heat transfer and electromagnetism to computer programming aspects.

Origins of the FEM are found in the early approximation of π by considering a sequence of inscribed polygons, although the method was formally introduced in 1960 by Clough.[27] In terms of the present day notation, each side of the polygon represented an element and as their number increases, the approximate values converge to the true one. Solving complex elasticity and structural analysis problems in civil and aeronautical engineering, for example wings and fuselages are treated as assemblies of stringers, skins and sear panels, further developed the method.

In 1851 Schellback in order to obtain a differential equation of a minimum surface area bounded by a specific closed curve, divided the surface into several triangles and used a finite difference expression to find the total discretized area.[11] The initial differential equation of a minimum surface area, was then replaced by a system of algebraic equations. Until the 1900's the behaviour of structural frameworks, composed of several bars arranged in a regular pattern, has been approximated by one of an isotropic elastic body.

Ritz, in 1909, developed an efficient method finding approximate solution of deformable solid mechanics problems. His approach referred to an approximation of an energy functional by known functions multiplied with unknown coefficients. Minimizing the functional in relation to each unknown leads to a system determining those coefficients, satisfying the given boundary conditions.

In 1915, Boris Grigoryevich Galerkin derived an advanced method for the numerical solution of differential equations. His method with piecewise polynomial

spaces is known as the finite element method. Technological advancements, further developed Galerkin's method. The approach traces back to variational principles introduced by several mathematicians, such as Leibniz, Euler, Lagrange, Dirichlet, and many others. Hrenikoff, in 1941, introduced the framework method. In this approach he replaced an elastic medium with a system of sticks and rods.

The FEM was introduced in the 50s by structural engineers, especially in the aircraft industry, predicting stresses induced in aircraft wings, despite being independently proposed by Courant in 1943.[21] He introduced special linear functions over triangular regions, obtained by dividing the cross region and applying the method for the solution of torsional rigidity and hallow shaft. The latter introduced the Rayleigh–Ritz method. The functions introduced by Ritz, did not need to satisfy the boundary conditions. Courant's theory could not be implemented due to the current absence of computers. Significant contributions to FEM were made by Turner, in 1956.

FEM obtained its main advancement in the 60s and 70s through developments of, among others, J. H. Argyris and collaborators. Clough, in 1960, introduced the term used until today, "finite element" in.[3] The first FEM book was published in 1967, by Zienkiewicz and Cheung.[26] The main motive behind the wide spread of FEM was the handling of big volume of numerical solution by computers.[20]

In this section, the main focus is on the Galerkin FEM. As previously mentioned, any progress to FEM, regarding fluid mechanics applications, was significantly delayed due to nonlinear convection and solution instability originating from the element selection. In this section, we are analysing basic principals of FEM, where more details can be found in the textbooks by Brenner & Scott.[5] In the next section we discuss about the FEM for the Stokes and Navier–Stokes problems. Finally, we introduce the Discontinuous Galerkin (DG) FEM and the adaptive mesh refinement approach.

2. Finite Element Theory

2.1. *Basic concepts and definitions*

It is important to understand the basics of the finite element theory. Analysing the following simple example helps the reader to understand the path followed to create the weak form of the problem. We consider the one–dimensional boundary value problem,

$$\begin{cases} -\dfrac{d^2u}{dx^2} = f, \quad x \in (0,1) \\ u(0) = 0, \quad u'(1) = 0 \end{cases} \tag{1}$$

Multiplying both parts of the equations with a test function v, with $v(0) = 0$ and integrating by parts, we get,

$$(f, v) := \int_0^1 f(x)v(x)\ dx = \int_0^1 -u''(x)v(x)\ dx = -u'(x)v(x)|_0^1 + \int_0^1 u'(x)v'(x)\ dx =$$
$$= \int_0^1 u'(x)v'(x)\ dx := \alpha(u, v),$$

where $\alpha(u, v)$ is a bilinear form.

Definition 1 (Bilinear form). A bilinear form is a function $B : V \times V \to K$, where V is a vector space and K is a scalar field, that is linear in each argument separately,

1. $B(u + v, w) = B(u, w) + B(v, w)$ and $B(\lambda u, v) = \lambda B(u, v)$
2. $B(u, v + w) = B(u, w) + B(u, w)$ and $B(u, \lambda v) = \lambda B(u, v)$

Definition 2 (Square–integrable function). A square–integrable function is denoted as L^2 and is defined as, $f : [a, b] \to \mathbb{C}$, square–integrable on [a,b] $\iff$ $\int_a^b |f(x)|^2\ dx < \infty$

Taking into consideration the above informations a function space can be defined as a test space:

$$V = \{v \in L^2(0, 1) : \alpha(u, v) < \infty \text{ and v(0)=0}\} \tag{2}$$

and

$$u \in V \text{ such that } a(u, v) = (f, v),\ \forall v \in V, \tag{3}$$

where $L^2(0, 1)$ is the space of square integrable functions in $[0, 1]$.

The function v, which multiplies the PDE, is referred as "test function". The unknown function u, that needs to be approximated, is called "trial function".[5] The trial and test spaces, V and $\hat{V}$, are defined as,

$$V = \left\{v \in H^1(\Omega) : v = u_0 \text{ on } \partial\Omega\right\},$$
$$\hat{V} = \left\{v \in H^1(\Omega) : v = 0 \text{ on } \partial\Omega\right\},$$

where $H^1(\Omega)$ is a Hilbert space.

Definition 3 (Hilbert space). Hilbert space is a complex vector space, whose topology is defined using an inner–product. A Hilbert space example is, $L^2(0, 1)$, with inner-product $(\cdot, \cdot)$. Hilbert spaces are complete metric spaces.

Definition 4 (Sobolev space). Sobolev space is a vector space of functions equipped with a norm, that is a combination of L^p–norms of the function and its derivatives, up to a given order. We define the Sobolev spaces as,

$$W_p^k(\Omega) := \{f \in L^1_{loc}(\Omega) : ||f||_{W_p^k(\Omega)}\} < \infty$$

In the cases where, $p = 2$, Sobolev space is a Hilbert space.

The function v is an arbitrary function and has a natural interpretation in the setting of Hilbert spaces. For the linear case it is known that, if the weak form is $a(u,v) = (f,v)$, where $a(\cdot,\cdot)$ is bilinear, and $u \in C^2[0,1]$ and $f \in C^0[0,1]$ satisfy the weak form, then u also satisfies the strong form, with appropriate initial conditions.[5]

According to the Ritz–Galerkin approximation we have that, if $S \subset V$ is any finite dimensional subspace and we consider that (3) with V is replaced by S, we get,

$$u_S \in S \text{ such that } a(u_S, v) = (f,v),\ \forall v \in S. \tag{4}$$

With the above we can define a discrete scheme for approximating (1) and it has been proven that given $f \in L^2(0,1)$, the equation has a unique solution.

Let's consider the two–dimensional Dirichlet problem,

$$u_{xx} + u_{yy} = f,\ in\ \Omega,\ u = 0,\ \ on\ \partial\Omega, \tag{5}$$

where, $u = u(x,y)$, $f = f(x,y)$, Ω is a connected open region and $\partial\Omega$ is the boundary of Ω. The weak form of this problem is ,

$$(f,v) := \int_\Omega fv\ ds = -\int_\Omega \bigtriangledown u \cdot \bigtriangledown v := -\alpha(u,v), \tag{6}$$

where ∇ denotes the gradient and $\cdot$ denotes the dot product in the two–dimensional plane. Where $\alpha(u,v)$ can be turned into an inner product on a suitable space $H_0^1(\Omega)$ of once differentiable functions of Ω that are zero on $\partial\Omega$. Additionally, $v \in H_0^1(\Omega)$ which is a Hilbert space.

2.2. *Error Estimates*

Definition 5 (Energy norm).

$$||v||_E = \sqrt{a(v,v)}, \quad \forall v \in V. \tag{7}$$

A relationship between the energy norm and the inner product is,

$$|a(u,v)| \leq ||u||_E ||v||_E. \tag{8}$$

It's proven that,

$$||u - u_S||_E = \min\{||u - v||_E : v \in S\}. \tag{9}$$

The last equation is defined as the error estimator where u is the solution and u_s is the approximate solution.

Definition 6 ($L^2(0,1)$ norm).

$$\|v\| = (v,v)^{\frac{1}{2}} = \left(\int_0^1 v(x)^2 dx\right)^{\frac{1}{2}} \tag{10}$$

The size of the error $u - u_s$ in this norm has been proven to be,

$$\|u - u_S\| \leq \varepsilon \|u - u_S\|_E \leq \varepsilon^2 \|u''\| = \varepsilon^2 \|f\| \tag{11}$$

with ε being a small number. $||u - u_s||_E$ is of order ε whereas $||u - u_s||$ is of order ε^2. We could conclude that the $L^2(0,1)$ norm is weaker than the energy one.

2.3. *Piecewise Polynomial Spaces*

We introduce linear polynomials to construct the Galerkin FEM and for that purpose we should partition our domain. Let's consider a partition of $[0,1]$, e.g. $0 = x_0 < x_1 < ... < x_n = 1$, and S be the linear space of functions v,
$S = \{v : [0,1] \to \mathbb{R} : \text{v is continuous, } v|_{[x_n, x_{n+1}]} \text{ is linear polynomial for } i = 1, ..., n \text{ and } v(0) = 0\}$

For each $i = 1, ..., n$ we can define ϕ_i and $\phi_i(x_j) = \delta_{ij}$ = the Kronecker delta i.e:

$$\begin{cases} \phi_i(x) = \dfrac{x - x_{i-1}}{x_i - x_{i-1}}, & x \in [x_{i-1}, xi] \\ \phi_i(x) = \dfrac{x_{i+1} - x}{x_{i+1} - x_i}, & x \in [x_i, x_{i+1}] \\ \phi_i(x) = 0, \quad otherwise \end{cases}$$

- $\{\phi_i : 1 \leq \text{i} \leq \text{n}\}$ is a nodal basis from S and it's called the **nodal basis** of S. The set $\{\phi_i\}$ is linearly independent, and it is used to define the functions of a discrete space.
- $\{v(x_i)\}$ are the **nodal values** of function v
- $\{x_i\}$ are the **nodes**
- $v_I = \sum_{i=1}^{n} v(x_i)\phi_i$, for $v \in C^0([0,1])$ and $v_i \in S$, is the **interpolant** of v

Remark 1. If $v \in S \implies v = v_I$ since $v - v_I$ is linear on each $[x_{i-1}, x_i]$, and zero at the endpoints, then must be equal to zero.

Theorem 1. *If $h = max_{1 \leq i \leq n}(x_i - x_{i-1})$ then $||u - u_I||_E \leq CH||u''||$, for all $u \in V$, where C is independent of h and u. The proof can be found in.*[5]

The interpolant of a continuous function, f, for the space of all piecewise linear functions is defined as,

$$\sum_e \sum_{j=0}^{1} f(x_{i(e,j)})\phi_j^e \tag{12}$$

where,

- $i(e,j)$ denotes a numbering scheme called the **global-to-local index** and aims to convert the coordinates of each element into the interval of $[0,1]$. For example: in the interval $[x_{e-1}, x_e]$ for $e = 1, ..., n$ and $j = 0, 1$ where 0 corresponds to left end of the interval and 1 to the right one

$$i(e,j) = e + j - 1$$

- $\{\phi_j^e\}$ with $j = 0, 1$ are the basis functions for the linear functions, on the interval $I_e = [x_{e-1}, x_e]$

$$\phi_j^e(x) = \phi_j(\frac{x - x_{e-1}}{x_e - x_{e-1}})$$

as far as it concerns the bilinear form, $a(v, w)$,

$$a(v, w) = \sum_e a_e(v, w)$$

where,

$$\sum_e a_e(v, w) := \int_{I_e} v'w' \, dx = \frac{1}{(x_e - x_{e-1})} \int_0^1 \left(\sum_j v_{i(e,j)} \phi_j \right)' \left(\sum_j w_{i(e,j)} \phi_j \right)' \, dx =$$

$$= \frac{1}{(x_e - x_{e-1})} \begin{pmatrix} v_{i(e,0)} \\ v_{i(e,1)} \end{pmatrix}^t K \begin{pmatrix} w_{i(e,0)} \\ w_{i(e,1)} \end{pmatrix},$$

where K is the local stiffness matrix,

$$K_{i,j} := \int_0^1 \phi'_{i-1} \phi'_{j-1} \, dx \quad \text{for} i, j = 1, 2.$$

2.4. *An Application to the Duffing equation*

In this section we present an example, the Duffing equation, using the Galerkin FEM. The Duffing equation serves as one of the simplest mathematical models for describing the nonlinear behaviour. The equation is a 2nd order nonlinear ODE, with constant coefficients, and with a periodically forced function.

$$\begin{cases} \dfrac{d^2u}{dx^2} + \delta \dfrac{du}{dx} + \alpha u + \beta u^3 = \gamma \cos wt, \quad u = u(t), \quad t \in [0, 1] \\ u(0) = 0 \ \text{ and } \ \dot{u(1)} = 1. \end{cases} \tag{13}$$

The parameter α is the linear stiffness coefficient, and the parameter β represents the nonlinearity in the restoring force. If $\beta = 0$, the equation describes simple harmonic oscillation. Overall, the equation represents a nonlinear spring that does not obey Hooke's law. Initially, we will demonstrate the steps of utilizing FEM in this equation and then we will obtain numerical results.[15,19]

We discretize the domain of the equation into a small number of elements to highlight the numerical approach. We start this procedure by dividing the function into a small number of elements for presentation purposes (four elements, five nodes) in the domain $[0, 1]$. Let $\phi = \phi(x)$ be the basis or test function. For each element $e = 1, 2, 3, 4$, we have two nodes t_i and t_{i+1}.

$$\int_{t_i}^{t_{i+1}} \left(\ddot{u} + \delta \dot{u} + \alpha u + \beta u^3 \right) \phi \, dt - \int_{t_i}^{t_{i+1}} \gamma \phi \cos \omega \, dt = 0, \tag{14}$$

where ϕ_i and ϕ_{i+1} were defined earlier. Let,

$$\phi(x) = \sum_{j=1}^{2} \phi_j(t) \text{ and } u(t) = \sum_{i=1}^{2} \phi_i(t).$$

Introducing the basis functions into equation (13), where,

$$h = t_{i+1} - t_i, \tag{15}$$

the equation can be written as follows ,

$$\mathrm{k}_{\mathrm{ij}}^{\mathrm{e}} = \mathrm{g}_{\mathrm{i}}^{\mathrm{e}}$$

where k_{ij}^e is the stiffness matrix and it is given as,

$$\mathrm{k}_{\mathrm{ij}}^{\mathrm{e}} = \int_{s_i}^{s_{i+1}} \left(-\dot{\phi}_i, \dot{\phi}_j + \delta\phi_i\phi_j + \alpha\phi_i\phi_j + \beta\phi_i^3\phi_j \right) \mathrm{dt}$$

and

$$\mathrm{g}_{\mathrm{i}}^{\mathrm{e}} = \gamma \int_{t_i}^{t_{i+1}} \phi_j \cos\omega t dt - \phi_j \dot{u}|_{t_i}^{t_{i+1}}.$$

For a typical element the stiffness matrix is,

$$K^e = \begin{bmatrix} k_{11} & k_{12} \\ k_{21} & k_{22} \end{bmatrix}$$

The global system of matrices equals,

$$K = \begin{pmatrix} k_{11}^1 & k_{12}^1 & 0 & 0 & 0 \\ k_{21}^1 & k_{22}^1 + k_{11}^2 & k_{12}^2 & 0 & 0 \\ 0 & k_{21}^2 & k_{22}^2 + k_{11}^3 & k_{12}^3 & 0 \\ 0 & 0 & k_{21}^3 & k_{22}^3 + k_{11}^4 & k_{12}^4 \\ 0 & 0 & 0 & k_{21}^4 & k_{22}^4 \end{pmatrix}$$

The force and boundary integral vectors are given as,

$$F = \begin{pmatrix} F_1^1 \\ F_2^1 + F_1^2 \\ F_2^2 + F_1^3 \\ F_2^3 + F_1^4 \\ F_2^4 \end{pmatrix}, \quad G = \begin{pmatrix} G_1^1 \\ 0 \\ 0 \\ 0 \\ G_2^4 \end{pmatrix}.$$

Finally the system we obtain is,

$$KU = F + G, \text{ where U}= \begin{pmatrix} u_1 \\ u_2 \\ u_3 \\ u_4 \\ u_5 \end{pmatrix}.$$

Due to the essential boundary conditions, we already know that $u(0) = u_1$. We should not forget that the approximate solution is, $u_h = \sum_{i=1}^{n} u(t_i)\phi_i$, where $u(t_i) = u_i$ and $\phi_i(t) = \phi_i$. For the simple example of this study, the time discretization is, $t_1 = 0, \quad t_2 = 0,25, \quad t_3 = 0,5, \quad t_4 = 0,75, \quad t_5 = 1$.

For $u(0) = \dot{u}(0) = 0$, $f(t) = 0.2\cos t$, $\delta = 0$, $\alpha = 0.06$, γ=0.2, w=1 and $\beta = 0.0001$, the numerical solution is shown for $N = 120$ nodes (119 elements) and it is compared with the Runge–Kutta (RK) 4th order method for the same parameters, as depicted in Figure 1(A).[19,24] We can conclude that the FEM and RK numerical solutions, with these particular parameters, coincide.

For $u(0) = 1$, $\dot{u}(0) = 0$ and $f(t) = 0$ and all the other parameters as described above, we present the comparison between the exact solution and the corresponding numerical one, as shown in Figure 1(B).

$$\dot{u}(t) = \sqrt{\alpha + \frac{\beta}{2} - \alpha u^2 - \frac{\beta}{2}u^4}, \tag{16}$$

All the numerical results of this section were obtained with the help of MATLAB and Mathematica software packages.

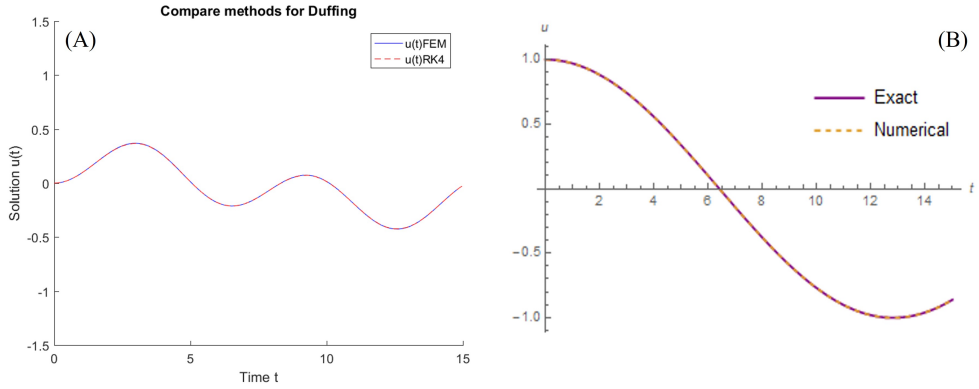

Fig. 1.: (A) Duffing equation with FEM and Runge–Kutta method for $u(0) = \dot{u}(0) = 0$, $f(t) = 0.2\cos(\omega t)$, $\delta = 0$, $\alpha = 0.06$, $\gamma = 0.2$, $\omega = 1$ and $\beta = 0.0001$. (B) Comparing exact and numerical solution for the Duffing equation for $u(0) = 1, \dot{u}(0) = 0$, $f(t) = 0$, $\delta = 0$, $\alpha = 0.06$, and $\beta = 0.0001$.

The Stokes and Navier–Stokes Problems

3. The Stokes Problem

The linear Stokes equations are the limiting case for the Navier–Stokes equations, when Reynolds number, *Re*, tends to zero. Due to close relation with the non-linear Navier–Stokes equations, the Stokes equations have attracted substantial attention from several researchers. We study the stationary Stokes problem for an incompressible fluid. Ω is a bounded open set of $\mathbb{R}^n$ (where $n = 2, 3$) with regular boundary and $\mathbf{f}$ is a square integrable function on Ω. We seek a solution $(\mathbf{u}, p) \in H_0^1(\Omega)^2 \times (L^2(\Omega)/\mathbb{R})$ of the problem,[16,20]

$$\begin{cases} -\nu\Delta\mathbf{u} + \nabla p = \mathbf{f} \quad in\ \ \Omega, \\ \qquad div\,\mathbf{u} = 0 \quad in\ \ \Omega, \\ \qquad\quad \mathbf{u} = 0 \quad on\ \ \partial\Omega. \end{cases} \tag{17}$$

Where, $\mathbf{u} = (u, v)$ denotes the velocity vector, whereas $\mathbf{f} = (f_x, f_y)$ stands for the body force vector. Based on this problem, we will introduce the error estimates (*a priori* and *a posteriori*) and we briefly discuss about the uniqueness of the solution for this problem. Our goal is to extend these arguments for the non–stationary case.[4] Following the finite element analysis we obtain the following weak form,

$$\begin{cases} a\left(\mathbf{u}, \mathbf{v}\right) + b\left(p, \mathbf{v}\right) = \left(\mathbf{f}, \mathbf{v}\right), & \forall\ \mathbf{v} \in H_0^1(\Omega)^n,\ \mathbf{u} \in H_0^1(\Omega)^n, \\ b\left(\mathbf{u}, q\right) = a((u,p),(v,q)) = \int_\Omega \nabla \cdot uq\ \mathrm{d}\Omega = 0 & \forall\ q \in H^1(\Omega),\ p \in H^1(\Omega), \end{cases} \tag{18}$$

where, $a\left(\mathbf{u}, \mathbf{v}\right) = \displaystyle\int_\Omega \nu\nabla\mathbf{u}\ \nabla\mathbf{v}\ d\Omega$ and $b\left(p, \mathbf{v}\right) = \displaystyle\int_\Omega p\ \nabla\mathbf{v}\ d\Omega$.

Given the finite dimensional subspaces, $V_h \subset H^1(\Omega)^n$ and $Q_h \subset H^1(\Omega)$ the discrete form is,

$$\begin{cases} a\left(\mathbf{u}_h, \mathbf{v}_h\right) + b\left(p_h, \mathbf{v}_h\right) = \left(\mathbf{f}, \mathbf{v}_h\right), & \forall\ \mathbf{v}_h \in V_{0h},\ \mathbf{u}_h \in V_{0h}, \\ b\left(\mathbf{u}_h, q_h\right) = 0, & \forall\ q_h \in Q_h,\ p_h \in Q_h, \end{cases} \tag{19}$$

where, $V_{0h} = \{\mathbf{v}_h \in V_h : \mathbf{v}_h\ |_{\partial\Omega} = 0\}$.

We analysed two different cases for triangular and quadrilateral elements, based on the number of nodes on each element.[4] We focus only on the Taylor–Hood

method with six node triangular elements. The Taylor–Hood method utilizes second order polynomials for the velocity and first order polynomials for the pressure, at each element $(P_2 - P_1)$.

After finding a solution, for the problem under consideration, it is important to show that it is stable and how the input data affect it. This can be done using the inf–sup condition, the Ladyzhenskaya–Babuska–Brezzi (LBB) condition. This is a condition for saddle point problems. Convergence is ensured for most discretization schemes for positive definite problems but for saddle point problems there are still discretizations that are unstable, due to spurious oscillations.[22] In such cases a better approach is the local adaptation of the computational grid, briefly described in a next section.[17] To further discuss for the LBB condition, we introduce the following theorem.

Theorem 2. *If Ω is polygonal and $\Omega_h = \Omega$, $\Omega_h = \bigcup_i T_i$, where T_i are the triangles and h defines the length of greatest triangle side. If all triangles have at least one vertex which is not on $\partial\Omega$, and if V_h, Q_h are chosen as in the Taylor–Hood method, then there exists a constant C, independent of h, such that,*

$$sup_{\mathbf{v}_h \in V_{0h}} \frac{(\mathbf{v}_h, \nabla q_h)}{(\mathbf{v}_h, \mathbf{v}_h)^{\frac{1}{2}}} \geq C \left(\nabla q_h, \nabla q_h\right)^{\frac{1}{2}}, \quad \forall q_h \in Q_h. \tag{20}$$

This theorem follows the idea of the LBB condition, the proof depends on the choice of the elements and it can be found in.[4] An important questions in solving such a problem is that of existence and uniqueness of the solution of the problem. In this case, we focus on the discrete form of the problem under consideration, e.g. the equation (19) where we can ensure the previous with the following theorem.[4]

Theorem 3. *Under the conditions of the previous theorem, theorem 2, the discrete form, equation* (19)*, has a unique solution $(\mathbf{u}_h, p_h)$ in $V_{0h} \times (Q_h/\mathbb{R})$.*

In the next section, we introduce and discuss error estimates of the Stokes problem.

3.1. *A Priori Error Estimates*

The *a priori* error estimates express the error in terms of the regularity of the exact unknown solution. They provide important information about the order of convergence of a FEM. *A posteriori* error estimates express the error in terms of computable quantities, such as the residual error and the solution of an auxiliary dual problem. They contribute to the adaptation of the computational grid, as described in a next section.[17] A theorem that provides *a priori* error estimates for the discrete form of the stationary Stokes problem using Taylor-Hood elements $(P_2 - P_1)$ is as follows.

Theorem 4. *Let Ω be a polygon, and $\Omega_h = \Omega$, for all h. We assume that each element of $\mathcal{T}_h$ (set of triangles) has at least one vertex not on the boundary. Then*

the following inequalities are valid,

$$\|\nabla(\mathbf{u}-\mathbf{u}_h)\|_0 \leqslant h^2 K\left(\|\mathbf{u}\|_{H^3(\Omega)^N}+\|p\|_{H^2(\Omega)/R}\right)$$
$$\|\nabla(p-p_h)\|_0 \leqslant hK\left(\|\mathbf{u}\|_{H^3(\Omega)^N}+\|p\|_{H^2(\Omega)/R}\right)$$

Similar inequalities can be found in the case where we have quadrilaterals.[4]

3.2. *The Backward Facing Step Problem*

The backward facing step (BFS) is a "test problem" widely known for its application on internal flows. In this problem, flow separation is caused due to sudden changes in the geometry. This creates a recirculation zone close to the step wall, and downstream a reattachment point. In a two–dimensional BFS geometry, the fluid flow can be distinguished into three regions, the shear layer, the separation bubble and the reattachment zone.[1,6]

Due to the adverse pressure gradient that develops in the thin shear layer, the characteristics of a BFS flow begin with an upstream boundary layer that separates at the edge of the backward facing step. The region where the shear layer develops is referred to as the shear layer region. This flow causes the formation of a recirculation zone, which is located between the shear layer and the adjacent wall. Eventually, the shear layer curves down towards the wall and reattaches at the so called reattachment point. The horizontal distance between the step and the reattachment point is defined as the "reattachment length". Due to the oscillatory motion of the shear layer, the reattachment length is unsteady. Consequently, the reattachment point spreads within a zone, called reattachment zone.[1,6] In this problem the flow parameters of interest are,

$$\begin{cases} \text{u= horizontal velocity component, v= vertical velocity component,} \\ \text{L= length, h= the step height, H= the whole height,} \\ \mu = \text{viscosity}, \rho = \text{density}, \end{cases}$$

with a typical set of boundary conditions, as shown in equation (21),

$$\begin{aligned} u &= u_0 \text{ on } \Gamma_D, \\ \nabla u \cdot n + pn &= g \text{ on } \Gamma_N, \end{aligned} \tag{21}$$

where,

- Γ_D are the **Dirichlet** conditions or the essential boundary conditions ,
- Γ_N are the **Neumann** conditions or the natural boundary conditions .

For further analysis, it is easier to write equations (17) to the following form for finding $(u,p) \in W$ such that,

$$a((\mathbf{u},p),(\mathbf{v},q)) = L(\mathbf{v},q)$$

for all $(\mathbf{v}, q) \in W$, where

$$a((\mathbf{u}, p), (\mathbf{v}, q)) = \int_\Omega \nabla\mathbf{u} \cdot \nabla\mathbf{v} - \nabla \cdot \mathbf{v}p + \nabla \cdot \mathbf{u}q \, \mathrm{d}x,$$
$$L(\mathbf{v}, q) = \int_\Omega \mathbf{f} \cdot \mathbf{v} \, \mathrm{d}x + \int_{\partial\Omega_N} g \cdot \mathbf{v} \, \mathrm{d}s.$$

The space W is a mixed (product) function space, $W = V \times Q$, such that $u \in V$ and $q \in Q$. We will use the Galerkin FEM to analyse the velocity and pressure on this test problem. Figure 2(A) shows the domain Ω and the dimensions of the backward facing step. Figure 2(B) depicts the computational mesh.

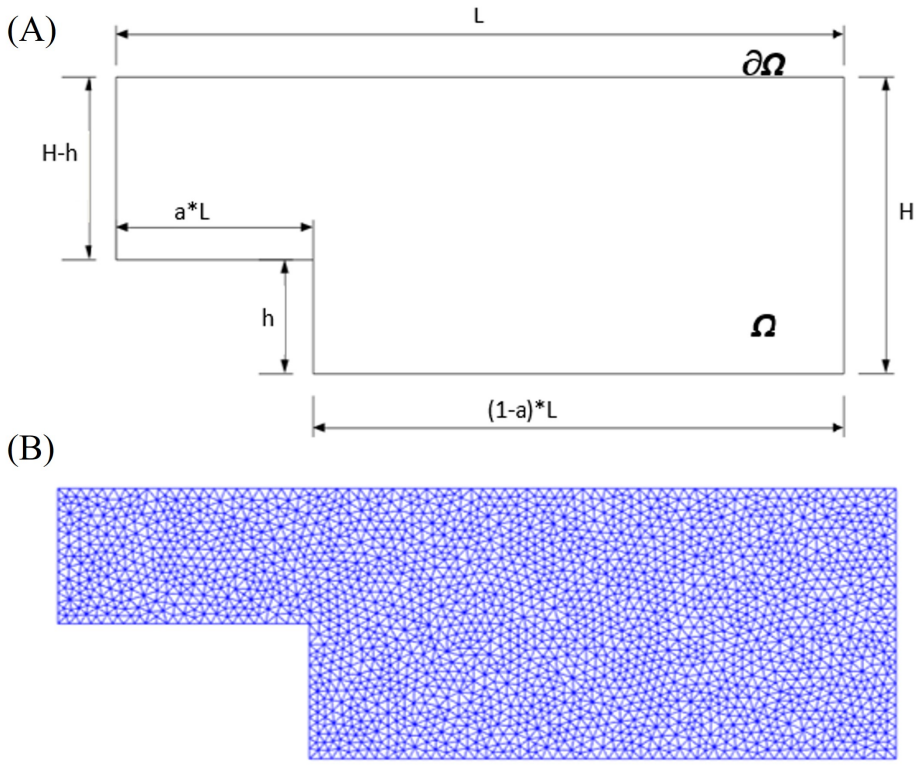

Fig. 2.: (A) The domain Ω and the dimensions of the backward step. (B) The computational mesh composed of approximately 6060 elements.

The numerical results are shown in Figure 3(A). The figure depicts the velocity magnitude for the backward facing step problem. We also present the streamlines in the domain to visualize the recirculation zone close to the wall. It is observed that the maximum velocity is at the entrance of the channel and the velocity drops rapidly as the domain expands. In Figure 3(B) we visualize the pressure field with

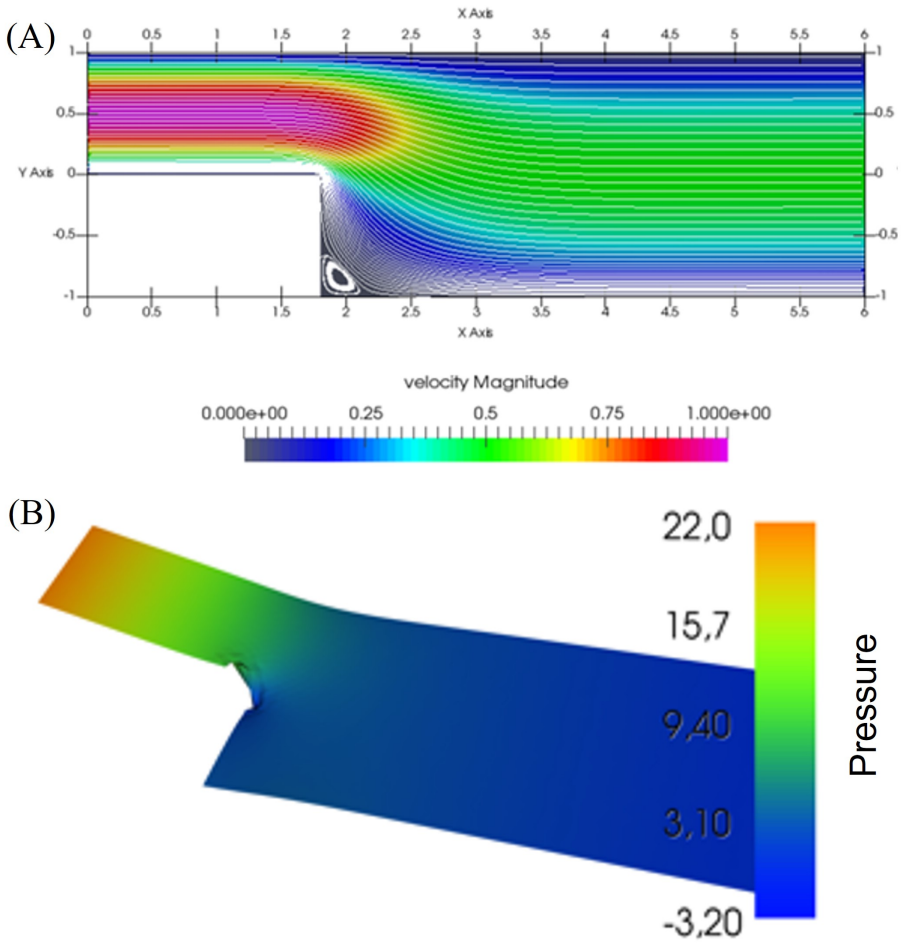

Fig. 3.: (A) The velocity magnitude of the Stokes equation on the backward step problem. (B) The pressure of the Stokes equation on the backward facing step problem.

the classical Galerkin FEM. It can be observed that the pressure field is relatively smooth using the Taylor–Hood elements.

4. The Navier–Stokes Problem

Most of every real situation in fluid flows is characterized by the Navier–Stokes equations that are the model of nonlinear PDEs, so it is recognizable the importance to solve this particular equation. Because of the nonlinearity of the problems that are described by the Navier–Stokes equations, an exact solution is impossible to be obtained. However, it is very useful to describe and analyse the physics of fluid flow

problems and also more complex materials if these equations can be solved. The FEM constitutes an effective way to find a numerical solution to these equations.

The time–dependent and incompressible Navier–Stokes equations are given as,

$$\begin{aligned} \frac{\partial \boldsymbol{u}}{\partial t} + (\boldsymbol{u}\cdot\nabla)\boldsymbol{u} - \nu\Delta\boldsymbol{u} + \nabla p = \boldsymbol{f} \quad & \text{in } \Omega\times(0,T) \\ \operatorname{div}\boldsymbol{u} = 0 \quad & \text{in } \Omega\times(0,T) \\ \boldsymbol{u} = \boldsymbol{0} \quad & \text{on } \partial\Omega\times(0,T) \\ \boldsymbol{u}(\cdot,0) = \boldsymbol{u}_0 \quad & \text{in } \Omega \end{aligned} \tag{22}$$

Where, $\boldsymbol{u}$ is the velocity field, p is the zero–mean pressure, $\boldsymbol{f}$ is an external force field, and ν is the kinematic viscosity. These equations, equations (22), describe an incompressible fluid flow in Ω. Compared to the Stokes equations we have here to deal with an additional nonlinearity and a time derivative. To obtain the weak formulation, we multiply the momentum equations with a test function, $\boldsymbol{v}$, defined in a suitable space V, and integrating both members with respect to the domain Ω,

$$\int_\Omega \frac{\partial \boldsymbol{u}}{\partial t}\cdot\boldsymbol{v} - \int_\Omega \nu\Delta\boldsymbol{u}\cdot\boldsymbol{v} + \int_\Omega (\boldsymbol{u}\cdot\nabla)\boldsymbol{u}\cdot\boldsymbol{v} + \int_\Omega \nabla p\cdot\boldsymbol{v} = \int_\Omega \boldsymbol{f}\cdot\boldsymbol{v} \tag{23}$$

Remark 2. Integrating by parts and using Gauss' divergence theorem,

$$-\int_\Omega \nu\Delta\boldsymbol{u}\cdot\boldsymbol{v} = \int_\Omega \nu\nabla\boldsymbol{u}\cdot\nabla\boldsymbol{v} - \int_{\partial\Omega}\nu\frac{\partial\boldsymbol{u}}{\partial\hat{\boldsymbol{n}}}\cdot\boldsymbol{v}$$

$$\int_\Omega \nabla p\cdot\boldsymbol{v} = -\int_\Omega p\nabla\cdot\boldsymbol{v} + \int_{\partial\Omega} p\boldsymbol{v}\cdot\hat{\boldsymbol{n}}$$

Using these relations the (23) is rearranged to,

$$\int_\Omega \frac{\partial u}{\partial t}\cdot\boldsymbol{v} + \int_\Omega \nu\nabla\boldsymbol{u}\cdot\nabla\boldsymbol{v} + \int_\Omega (\boldsymbol{u}\cdot\nabla)\boldsymbol{u}\cdot\boldsymbol{v} - \int_\Omega p\nabla\cdot\boldsymbol{v} = \int_\Omega \boldsymbol{f}\cdot\boldsymbol{v} + \int_{\partial\Omega}\left(\nu\frac{\partial\boldsymbol{u}}{\partial\hat{\boldsymbol{n}}} - p\hat{\boldsymbol{n}}\right)\cdot\boldsymbol{v} \quad \forall\boldsymbol{v}\in V \tag{24}$$

In a similar manner, we multiply the continuity equation with a test function q, belonging to a space Q and integrated in the domain Ω,

$$\int_\Omega q\nabla\cdot\boldsymbol{u} = 0. \quad \forall q\in Q$$

The space functions are chosen as,

$$V = \left[H_0^1(\Omega)\right]^d = \left\{v\in\left[H^1(\Omega)\right]^d : \quad v = 0 \text{ on } \Gamma_D\right\}$$

$$Q = L^2(\Omega)$$

Due to the set of boundary conditions,

$$u = 0 \text{ on } \Gamma_D$$

$$\nabla u\cdot n + pn = g \text{ on } \Gamma_N$$

the integral on the boundary can be written as,

$$\int_{\partial\Omega}\left(\nu\frac{\partial\boldsymbol{u}}{\partial\hat{\boldsymbol{n}}} - p\hat{\boldsymbol{n}}\right)\cdot\boldsymbol{v} = \int_{\Gamma_D}\left(\nu\frac{\partial\boldsymbol{u}}{\partial\hat{\boldsymbol{n}}} - p\hat{\boldsymbol{n}}\right)\cdot\boldsymbol{v} + \int_{\Gamma_N}\left(\nu\frac{\partial\boldsymbol{u}}{\partial\hat{\boldsymbol{n}}} - p\hat{\boldsymbol{n}}\right)\cdot\boldsymbol{v} = \int_{\Gamma_N}\boldsymbol{g}\cdot\boldsymbol{v}$$

where,

- $\int_{\Gamma_D} \left(\nu \frac{\partial \boldsymbol{u}}{\partial \hat{\boldsymbol{n}}} - p\hat{\boldsymbol{n}}\right) \cdot \boldsymbol{v} = 0$
- $\int_{\Gamma_N} \left(\nu \frac{\partial \boldsymbol{u}}{\partial \hat{\boldsymbol{n}}} - p\hat{\boldsymbol{n}}\right) \cdot \boldsymbol{v} = -g \cdot v$

Eventually, the weak form of the Navier–Stokes equations is expressed as,

$$\begin{cases} \int_\Omega \dfrac{\partial \boldsymbol{u}}{\partial t} \cdot \boldsymbol{v} + \displaystyle\int_\Omega \nu \nabla \boldsymbol{u} \cdot \nabla \boldsymbol{v} + \int_\Omega (\boldsymbol{u} \cdot \nabla)\boldsymbol{u} \cdot \boldsymbol{v} - \int_\Omega p \nabla \cdot \boldsymbol{v} = \int_\Omega \boldsymbol{f} \cdot \boldsymbol{v} + \int_{\Gamma_N} \boldsymbol{g} \cdot \boldsymbol{v} \quad \forall \boldsymbol{v} \in V \\ \int_\Omega q \nabla \cdot \boldsymbol{u} = 0, \quad \forall q \in Q. \end{cases}$$

Existence and uniqueness of the solution of the problem is discussed in the following theorem,

Theorem 5. *If $f \in \left[L^2(0,T;V')\right]^d$ and $u_0 \in H$, there exists a weak solution to the Navier–Stokes equations, equation* (22)*, that satisfies,*[23]

$$\boldsymbol{u} \in L^2(0,T;\boldsymbol{V}) \cap L^\infty(0,T;\boldsymbol{H})$$

where,

$$\boldsymbol{V} = \left\{ \boldsymbol{v} \in \left[H_0^1(\Omega)\right]^d : \operatorname{div} \boldsymbol{v} = 0 \right\},$$
$$\boldsymbol{H} = \left\{ \boldsymbol{v} \in \left[L_0^2(\Omega)\right]^d : \operatorname{div} \boldsymbol{v} = 0 \right\}.$$

In the case of space dimension $d = 2$, this solution is unique and

$$\boldsymbol{u} \in C(0,T;\boldsymbol{H}),$$
$$\boldsymbol{u}' \in L^2\left(0,T;\boldsymbol{V}'\right).$$

In three–dimensions ($d = 3$) uniqueness is an open question.

4.1. *An Application to the Poiseuille flow*

In this section, we study the incompressible Navier–Stokes flow between two long parallel plates, with no–slip condition on both walls which are spaced apart in height $2h$ (Poiseuille flow). We assume a constant flow, with density ρ and viscosity μ to be constant. Fluid is introduced with a parabolic velocity profile at the inlet of the domain, $u(y) = 4\,y\,(y-1)$. With the aforementioned assumptions, we note that,

$$\begin{cases} y = -h \text{ or } y = +h, \\ u(x,y) = 0,\ v(x,y) = 0,\ F_x = F_y = 0. \end{cases}$$

With the above boundary conditions we obtain that,

$$\frac{\partial u}{\partial x} = 0 \text{ i.e.} u = u(y). \tag{25}$$

$$\rho u_x \frac{\partial u_x}{\partial x} = -\frac{\partial p}{\partial x} + \mu \left(\frac{\partial^2 u_x}{\partial x^2} + \frac{\partial^2 u_x}{\partial y^2} \right) \tag{26}$$

$$-\frac{\partial p}{\partial y} = 0 \text{ i.e.} p = p(x). \tag{27}$$

Thus, we obtain,

$$\frac{\partial p}{\partial x} = c = \mu \frac{d^2 u}{dy^2} \tag{28}$$

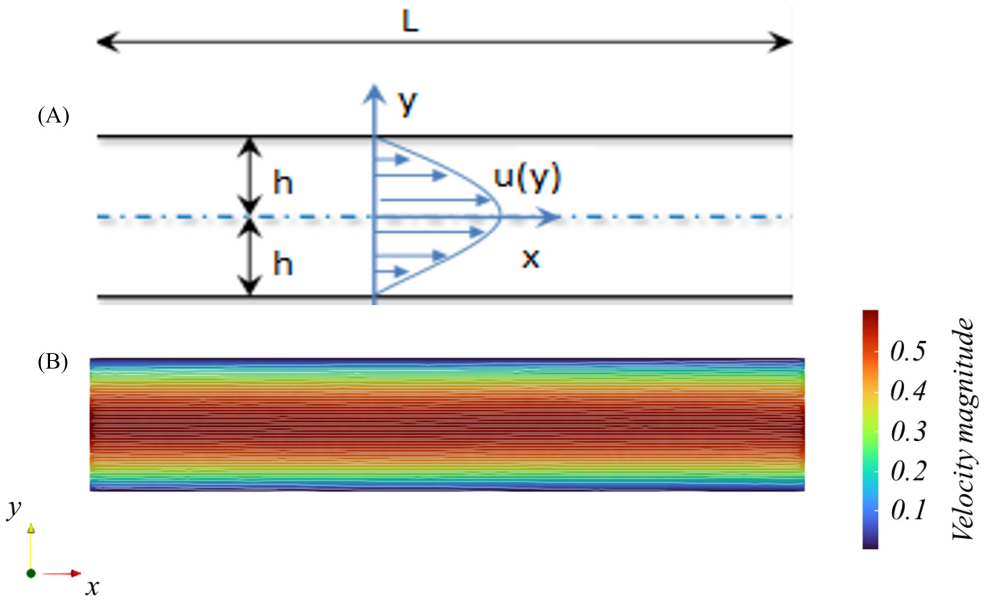

Fig. 4.: (A) Fluid flow schematics between two parallel plates providing a parabolic profile, known as Poiseuille flow. (B) The numerical solution of the Poiseuille flow, using FEM and the software package FEniCS.

Solving the differential equation (26), and applying the boundary conditions yields to the analytical solution of the problem under consideration, that is a parabolic profile as expected,

$$u(y) = -\frac{c}{2\mu}(h^2 - y^2). \tag{29}$$

The velocity has a parabolic profile, as shown in equation (29). If $c > 0$ the maximum velocity value is at the centre of the domain, for $y = 0$ and $u_{max} = -\frac{ch^2}{2\mu}$, that indicates a favourable pressure drop within this region, given by $\frac{\partial p}{\partial x} = c_2 = -\frac{ch^2}{2\mu}$ and depicted in the schematic of Figure 4(A).

We obtain the analytical solution for the Poiseuille problem, as shown in equation (29). Additionally, solving the same problem with the FEM and the software

package FEniCS we obtain the same parabolic profile, as shown in Figure 4(B). The FEM results were obtained for a computational mesh of approximately 2754 triangular elements. The maximum velocity is at the centreline of the domain and at the plates we have zero velocity, no-slip condition, as also discussed for the analytical solution.

Discontinuous and Adaptive FEM

5. The Discontinuous Galerkin FEM

The discontinuous Galerkin (DG) FEMs are used in the numerical analysis of differential equations. They serve as an improvement to both the finite element and finite volume methods and they apply to a plethora of problems in fluid dynamics. The basis functions used, are discontinuous. These methods, allowing discontinuities, apply with great flexibility and benefits, handling complex geometries, irregular meshes, and polynomial approximations of different degree in each element.[7] The discontinuous methods are distinguished from the continuous ones in integrating flux terms over interior faces.

The DG methods first arose in solving PDEs in the early 70s, with continuous improvements on elliptic problems, through out the decade.[2,13] In the 90s, extensions of the DG method, dealt with the compressible flow and nonlinear hyperbolic conservation laws. The analysis and development of such methods, is a topic of active research.[8]

The following example, provides an approximate solution u_h of an ODE using the DG FEM. Consider the initial–value problem,[7]

$$\begin{cases} \dfrac{d}{dt}u(t) = f(t)u(t), \;\; t \in (0,T), \\ u(0) = u_0. \end{cases} \tag{30}$$

Initially, we divide the interval $I := (0,T)$, into subintervals $I_i := (t_i, t_{i+1})$, for $i = 0, 1, ..., N-1$. Next, we seek the approximate solution u_h, which on the interval I_i, is a polynomial of degree at most k^i, requiring that,

$$-\int_{I_i} u_h(s)\frac{d}{ds}v(s)\,ds + \hat{u}_h v|_{t_i}^{t_{i+1}} = \int_I u(s)f(s)v(s)\,ds, \tag{31}$$

for polynomials v of degree at most k^i, where the quantity $\hat{u}_h$ is ,

$$\hat{u}_h := \begin{cases} u_0, \;\; if \;\; t_i = 0 \\ \lim_{\varepsilon\to 0} u_h(t_i - \varepsilon), \;\; otherwise. \end{cases}$$

Our goal is to find a suitable definition of the *numerical trace*, $\hat{u_h}$, using discontinuous approximations, u_h, and applying the Galerkin weak formulation. The DG FEMs are *consistent* methods. So, when replacing the approximate solution u_h with the exact solution u, in the weak formulation of the equation (31), the equation is satisfied. That can be applied if $\widehat{u} = u$.

Multiplying the ODE with u and integrating on the domain $(0, T)$, we get,

$$\frac{1}{2}u^2(T) - \frac{1}{2}u_0^2 = \int_0^T f(s)u^2(s)ds.$$

Substituting $v = u_h$ in the weak formulation, equation (31), and integrating by parts we obtain the following,

$$\sum_{i=0}^{N-1}\left(-\frac{1}{2}u_h^2 + \hat{u}_h u_h\right)\Big|_{t_i}^{t_{i+1}} = \frac{1}{2}u_h^2\left(T^-\right) + \Theta_h\left(T'\right) - \frac{1}{2}u_0^2 = \int_0^T f(s)u_h^2(s)ds,$$

where,

$$\Theta_h(T) = -\frac{1}{2}u_h^2\left(T^-\right) + \sum_{i=0}^{N-1}\left(-\frac{1}{2}u_h^2 + \hat{u}_h u_h\right)\Big|_{t_i}^{t_{i+1}} + \frac{1}{2}u_0^2.$$

The stability is gained when $\Theta_h(T) \geq 0$, so we set,

$$u_h(t) = u_0, \quad t < 0.$$

We further introduce the following definitions,

Definition 7. We define as the average quantity of the discrete function u_h the, $\{u_h\} = \frac{1}{2}\left(u_h^- + u_h^+\right)$. Additionally, we define the difference of the discrete function u_h on the faces of each element as, $[u_h] = u_h^- - u_h^+$.

Definition 8. We define the limit of the discrete function u_h at the faces as, $u_h^{\pm}(t) = \lim_{\varepsilon\to 0} u_h(t \pm \varepsilon)$.

Remark 3. The above definitions yields to the following equation,

$$\left[u_h^2\right] = 2\left\{u_h\right\}\left[u_h\right].$$

Taking into consideration the above definitions,

$$\begin{aligned}\Theta_h(T) =& -\frac{1}{2}u_h^2\left(T^-\right) + \left(-\frac{1}{2}u_h^2\left(T^-\right) + \hat{u}_h(T)u_h\left(T^-\right)\right) + \sum_{i=1}^{N-1}\left(-\frac{1}{2}\left[u_h^2\right] + \hat{u}_h\left[u_h\right]\right)(t_i)\\ &- \left(-\frac{1}{2}u_h^2\left(0^+\right) + \widehat{u}_h(0)u_h\left(0^+\right)\right) + \frac{1}{2}u_0^2\\ =& \left(\widehat{u}_h(T) - u_h\left(T^-\right)\right)u_h\left(T^-\right) + \sum_{i=1}^{N-1}\left(\left(\widehat{u}_h - \{u_h\}\right)[u_h]\right)(t_i)\\ &- \left(\widehat{u}_h(0) - u_0\right)u_h\left(0^+\right) + \frac{1}{2}\left[u_h\right]^2(0)\end{aligned}$$

Based on the above, we have for the $\widehat{u}_h$,

$$\widehat{u}_h\left(t_i\right) = \begin{cases} u_0, & \text{if } t_i = 0 \\ \left(\{u_h\} + C^i\left[u_h\right]\right)\left(t_i\right), & \text{if } t_i \in (0,T) \\ u_h(T-), & \text{if } t_i = T \end{cases}$$

$C^i \geq 0$ and $C^0 = 1/2$,

$$\Theta_h(T) = \sum_{i=0}^{N-1} C^i \left[u_h\right]^2 \left(t_i\right) \geq 0.$$

The accuracy of the DG method depends on the choice of C^i. The order of the DG method at the points t_i is $2k+1$, if we take $C^i = \dfrac{1}{2}$. For $C^i = 0$, it can be proven that the order of the DG method is $2k+2$.[10,13] However, for $C^i \equiv 1/2$, DG methods are consistent and stable. As a consequence, we can handle different types of approximations in different elements.

For higher order problems, the first step is the discretization of the domain of interest in triangles, denoting by $\mathcal{T}$, such triangulation. We further seek a discontinuous approximate solution u_h, that in each element K, of the triangulation $\mathcal{T}$, belongs to space $V(K)$.[10,13]

5.1. *Application to the Poisson and Stokes Equations*

Next, we present the methodology of applying the Discontinuous Galerkin (DG) to the Poisson and the Stokes equations.[18] For the Poisson equation, we consider a DG FEM. For this problem we apply Dirichlet boundary conditions,

$$\begin{aligned} -\Delta u &= f \quad \text{in } \Omega, \\ u &= u_D \quad \text{on } \partial\Omega. \end{aligned}$$

Next we rewrite the Poisson equation to the weak form,

$$\int_\Omega -(\Delta u)\cdot v dx = \int_\Omega f v dx$$

Assume that we have a mesh $\mathcal{T}$ of Ω with cells $\{K\}$ and split the left integral into sum over cell integrals:

$$\sum_{K\in\mathcal{T}} \int_K -(\Delta u)\cdot v \, \mathrm{d}x = \int_\Omega f v \, \mathrm{d}x$$

Now integrating by parts,

$$\sum_{K\in\mathcal{T}} \int_K \nabla u \cdot \nabla v \, \mathrm{d}x - \sum_{K\in\mathcal{T}} \int_{\partial K} \nabla u \cdot n v \, \mathrm{d}s = \int_\Omega f v \, \mathrm{d}x.$$

Before introducing the DG method, it is necessary to point out the definitions relevant to this method,[9]

Definition 9 (Average and Jump operator). We define the average quantity of the function v as, $\langle v \rangle = \frac{1}{2}\left(v^+ + v^-\right)$. We also define the difference, or jump, of the function v on the element faces as, $[vn] = v^+ n - v^- n$ in Ω and $[vn] = vn$ on $\partial\Omega$.

Definition 10 (Jump identity). We define for the functions u and v, the jump identity as, $[uv] = [u]\langle v\rangle + \langle u\rangle[v]$ in Ω

We consider a DG formulation to approximate the problem. For this formulation, the approximation space is made of piecewise discontinuous polynomials, such as,

$$V = \left\{ v \in L^2(\Omega) : v|_K \in Q_p(K) \text{ for all } K \in \mathcal{T} \right\},$$

where $\mathcal{T}$ is the set of all cells K of the mesh, and $Q_p(K)$ is a polynomial space of p–degree defined on a cell K. We need to introduce appropriate notation, in order to write the weak form of the problem under consideration. The sets of interior and boundary facets associated with the mesh $\mathcal{T}$, are denoted as $\mathcal{F}_i$ and $\mathcal{F}_e$, respectively. With v^+, and v^- being the restrictions of $v \in V$ to the cells K^+, K^- that share the same interior facet in $\mathcal{F}_i$ and n^+, n^-, the facet outward unit normals from either the perspective of K^+ and K^-, respectively.[9]

With the above introduced notation, the weak form associated with the interior penalty formulation for the Poisson equation is presented as,

$$\begin{aligned} a(v,u) = & \sum_{K\in\mathcal{T}} \int_K \nabla v \cdot \nabla u \, \mathrm{d}K \\ & - \sum_{K\in\mathcal{F}_e} \int_K v(\nabla u \cdot n)\mathrm{d}K - \sum_{K\in\mathcal{F}_e} \int_K (\nabla v \cdot n)u \, \mathrm{d}K + \sum_{K\in\mathcal{F}_e} \frac{\alpha}{h} \int_K v \cdot u \, \mathrm{d}K \\ & - \sum_{K\in\mathcal{F}_i} \int_K [vn] \cdot \langle \nabla u\rangle \mathrm{d}K - \sum_{K\in\mathcal{F}_i} \int_K \langle \nabla v\rangle \cdot [un]\mathrm{d}K + \sum_{K\in\mathcal{F}_i} \frac{\alpha}{h} \int_K [vn] \cdot [un]\mathrm{d}K, \end{aligned}$$

and the right–hand side is presented as,

$$L(v) = \int_\Omega vf \, \mathrm{d}\Omega.$$

Remark 4. We provide the following equation for the element boundary,

$$\begin{aligned} \sum_{K\in\mathcal{T}} \int_{\partial K} \nabla u \cdot nv \, \mathrm{d}s = & \sum_{K\in\mathcal{F}_i} \int_K \left(\nabla u^+ \cdot n^+ v^+ + \nabla u^- \cdot n^- v^- \right) \mathrm{d}s \\ & + \sum_{K\in\mathcal{F}_e} \int_K \nabla u \cdot nv \, \mathrm{d}s \end{aligned}$$

Remark 5. The terms, $\sum_{K\in\mathcal{F}_e} \frac{\alpha}{h} \int_K v \cdot u \, \mathrm{d}K$ and $\sum_{K\in\mathcal{F}_i} \frac{\alpha}{h} \int_K [vn] \cdot [un]\mathrm{d}K$, are artificially added in the formulation. The constant α, is a stabilization parameter. This parameter should be chosen large enough such as the bilinear form $a(\cdot,\cdot)$ is stable and continuous. Where, h, is a measure for the average of the mesh size defined as $h = (h^+ + h^-)/2$, for the two neighbouring cells K^+ and K^-, with the given interior facet.

When applying the above formulation, e.g. the DG FEM, using the software program FeniCS for the Poisson equation, we obtain the results shown in Figure 5. In the domain we apply homogeneous Dirichlet conditions on the boundary. Internally a Gaussian distribution is applied for the source term, defined by the function f, on the right–hand side of the Poisson equation, given by the expression,

$$f(x,y) = c\exp\left(-\frac{(x-\alpha)^2+(y-b)^2}{d}\right), \tag{32}$$

where, $c = 10.$, $\alpha = b = 0.5$ and $d = 0.02$.

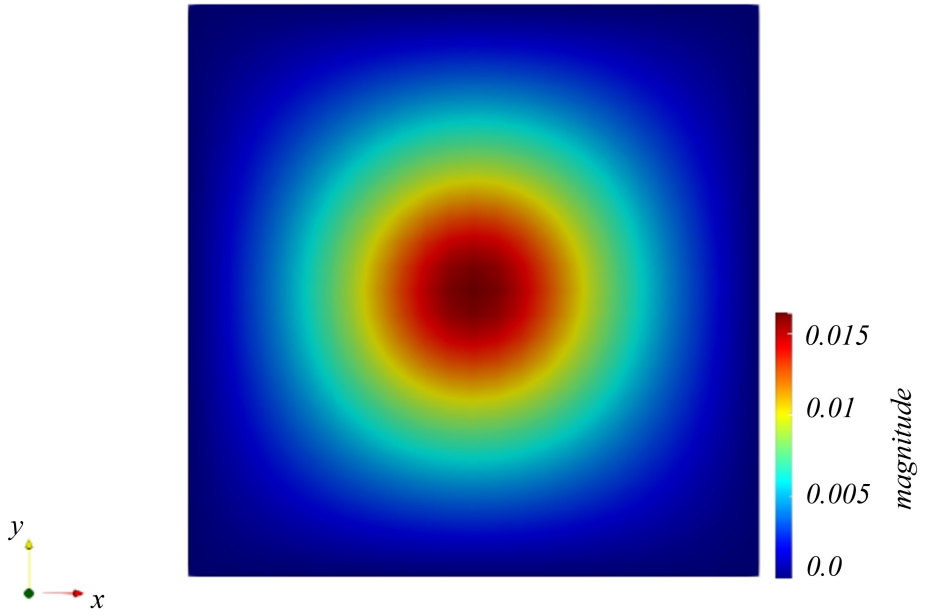

Fig. 5.: Numerical solution of the Poisson equation with DG FEM and homogeneous Dirichlet conditions.

Following the same methodology as before, we use DG FEM for the Stokes problem,

$$\begin{cases} -\nu\Delta\mathbf{u} + \nabla p = \mathbf{f} \text{ in } \Omega, \\ \mathbf{u} = 0 \text{ on } \partial\Omega. \end{cases}$$

Consider the function spaces V, equipped with discontinuous functions, and Q with continuous ones,

$$V = \left\{\boldsymbol{v} \in \left(L^2(\Omega)\right)^d : v_i \in P_k(K) \forall K \in \mathcal{T}, 1 \leq i \leq d\right\},$$
$$Q = \left\{q \in H^1(\Omega) : q \in P_j(K) \forall K \in \mathcal{T}\right\}.$$

We presented earlier the weak formulation,

$$a((\mathbf{u},p),(\mathbf{v},q)) = L(\mathbf{v},q)$$

for all $(\mathbf{v},q) \in W$, where,

$$a((\mathbf{u},p),(\mathbf{v},q)) = \int_\Omega \nu\nabla\mathbf{u}\cdot\nabla\mathbf{v} - \nabla p\cdot\mathbf{v} + \nabla q\cdot\mathbf{u}\ \mathrm{d}x,$$
$$L((\mathbf{v},q)) = \int_\Omega \mathbf{f}\cdot\mathbf{v}\ \mathrm{d}x + \int_{\partial\Omega_N} g\cdot\mathbf{v}ds.$$

The space W, is considered as a mixed (product) function space, $W = V \times Q$, such that, $u \in V$ and $q \in Q$.

In order to formulate the Stokes problem with the DG FEM, we consider both discontinuous functions, as well as, basis functions with varying polynomial orders. The particular bilinear and linear forms for the Stokes equation with DG method can be formulated as,

$$\begin{aligned}
a(\boldsymbol{v},q;\boldsymbol{u},p) = & \\
&\sum_{K\in\mathcal{T}}\int_K \nabla\boldsymbol{v}\cdot\nabla\boldsymbol{u}\mathrm{d}K + \sum_{K\in\mathcal{T}}\int_K \boldsymbol{v}\cdot\nabla p\ \mathrm{d}K - \sum_{K\in\mathcal{T}}\int_K \nabla q\cdot\boldsymbol{u}\mathrm{d}K \\
&+ \sum_{K\in\mathcal{F}_i}\int_K q[\boldsymbol{u}\cdot\boldsymbol{n}]\mathrm{d}T - \sum_{K\in\mathcal{F}_i}\int_K \nu[\boldsymbol{v}]\cdot\langle\nabla\boldsymbol{u}\rangle\mathrm{d}K \\
&- \sum_{K\in\mathcal{F}_i}\int_K \nu\langle\nabla\boldsymbol{v}\rangle\cdot[\boldsymbol{u}]\mathrm{d}K + \sum_{K\in\mathcal{F}_i}\int_K \nu\frac{\alpha}{h}[\boldsymbol{v}]\cdot[\boldsymbol{u}]\mathrm{d}K \\
&+ \sum_{K\in\mathcal{F}_e}\int_K q\boldsymbol{u}\cdot\boldsymbol{n}\mathrm{d}K - \sum_{K\in\mathcal{F}_e}\int_K \nu\boldsymbol{v}\cdot\nabla\boldsymbol{u}\mathrm{d}K \\
&- \sum_{K\in\mathcal{F}_e}\int_K \nu\nabla\boldsymbol{v}\cdot\boldsymbol{u}\mathrm{d}K + \sum_{K\in\mathcal{F}_e}\int_K \nu\frac{\alpha}{h}\boldsymbol{v}\cdot\boldsymbol{u}\mathrm{d}K
\end{aligned}$$

and the right–hand side of the Stokes problem is given as,

$$L(\boldsymbol{v},q) = \int_\Omega \boldsymbol{v}\cdot\boldsymbol{f}dx.$$

The above formulation is constructed in a same manner as the Poisson equation with the terms $\sum_{K\in\mathcal{F}_i}\int_K \nu\frac{\alpha}{h}[\boldsymbol{v}]\cdot[\boldsymbol{u}]\mathrm{d}K$ and $\sum_{K\in\mathcal{F}_e}\int_K \nu\frac{\alpha}{h}\boldsymbol{v}\cdot\boldsymbol{u}\mathrm{d}K$ being artificially added for the stability of the equation.

6. Adaptive Mesh Refinement FEM

The adaptive mesh refinement (AMR) is an approach for increasing the accuracy of the numerical solution in certain sensitive regions of the discretized domain. Numerical solutions, sometimes reveal accuracy problems to specific regions of the grid or mesh. However, some problems would be better suited if specific computational areas which needed precision could be refined only in the regions requiring the added precision rather than a uniform region. There are widely used methods that omit this problem, called Adaptive Finite Element Mesh Refinement methods (AFEM) with a range of applications to engineering problems. AFEM can be classified into three categories,[25]

- In the h-refinement AFEM, we use the same type of finite elements, but their sizes are continuously divided according to a geometric parameter such as the element length or diameter. Among the three categories referred, this is the simplest and more common one to use.
- In the p-refinement AFEM, we increase the order of the polynomial basis functions, but the mesh element size is kept the same.
- In r-refinement AFEM, we keep the number of mesh nodes and elements the same, but the nodes are relocated to problematic areas needed to be optimized.

These methods can be combined, such as the hp–refinement method. We can use the AFEM to obtain a numerical solution of the desired accuracy, with less computing time, since lower degrees of freedom are needed. For the h–type AFEM, the main concept is to determine the regions to insert the nodes, so as to balance the numerical errors of the FEM solution through a local *a posteriori* error estimate procedure. The *a posteriori* error estimation obtains an estimated error for each element. This plays an important role in guiding the refinement procedures for AFEM.

The process consists of calculating the error indicators for each element of the mesh. Then, a selected number of elements in the domain, e.g. the elements with the largest error indicators, are finally refined. This process is repeated several times until the termination conditions are satisfied. Such conditions could be the maximum refinement number or maximum nodes number in the mesh. The elements can be refined with several methods, such as by bisection, trisection, regular refinement or any combinations of these methods.[25]

More precisely, let's consider an *a posteriori* estimator for the Stokes problem. It can be shown that the discrete solution coincides with the continuous one. To define the Stokes reconstruction, we provide the definition of the Stokes reconstruction operator.[12] *A posteriori* error estimates express the error in terms of important quantities, such as the residual error equations and the solution of an auxiliary dual problem.[14] By using the classical Galerkin method, the FEM approximation

$u_h \in V^h$ is the solution of,

$$a\left(u_h, v\right) = L(v), \quad \forall v \in V^h.$$

The numerical error in the approximate solution u_h of u is defined as the function $e \in V$ such that,

$$e = |u - u_h|.$$

The residual errors are defined as $r(v)$, where,

$$\begin{gathered} r(v) = L(v) - a\left(u_h, v\right) = a(u, v) - a\left(u_h, v\right) = \\ a\left(u - u_h, v\right) \leqslant C \left\|u - u_h\right\|_V \|v\|_V, \quad v \in V. \end{gathered} \tag{33}$$

Furthermore,

$$\begin{gathered} \alpha \left\|u - u_h\right\|_V^2 \leqslant a\left(u - u_h, u - u_h\right) = \\ a\left(u, u - u_h\right) - a\left(u_h, u - u_h\right) = \\ L\left(u - u_h\right) - a\left(u_h, u - u_h\right) = r\left(u - u_h\right). \end{gathered} \tag{34}$$

Remark 6. We notice that the residual error $r(v)$ vanishes for all $v \in V^h$, i.e.,

$$r(v) = 0, \quad \forall v \in V^h.$$

This yields to the following orthogonality property,

$$a(e, v) = 0, \quad \forall v \in V^h$$

Combining (33), (34) yields to:

$$\alpha \left\|u - u_h\right\|_V \leqslant \|r\|_{V'} \leqslant C \left\|u - u_h\right\|_V \tag{35}$$

where $\|r\|_{V'} = \sup_{v \in V, v \neq 0} r(v)/\|v\|_V$.

The *a posteriori* error estimates, equation (35), relate the numerical error with the residuals.

The main objective of Goal–oriented error estimation is to evaluate the accuracy of FEM solutions in measures other than the energy norm.[14] In numerical applications, it is often necessary to control the error in a certain output functional $\mathcal{M} : V \to \mathbb{R}$ of the computed solution within a given tolerance $\varepsilon > 0$. Typical functionals are the quantities we are interested in. In such situations, one could ideally choose the finite element space $V_h \subset V$, such that, the finite element solution u_h satisfies,

$$\eta \equiv |\mathcal{M}(u) - \mathcal{M}\left(u_h\right)| \leqslant \varepsilon,$$

with minimal computational work. We assume that both the output functional and the variational problem are linear, but the analysis may be easily extended to the full nonlinear case. To estimate the error in the output functional, $\mathcal{M}$, we introduce an auxiliary dual problem, that is, find $z \in V^*$ such that,

$$a^*(z, v) = \mathcal{M}(v), \quad \forall v \in \hat{V}^*.$$

We note here that the functional $\mathcal{M}$, is introduced as data in the dual problem. The dual (adjoint) bilinear form, $a^* : V^* \times \hat{V}^* \to \mathbb{R}$ is defined by,

$$a^*(v, w) = a(w, v), \quad \forall (v, w) \in V^* \times \hat{V}^*.$$

The dual trial and test spaces are given by,

$$V^* = \hat{V},$$
$$\hat{V}^* = V_0 = \{v - w : v, w \in V\},$$

The definition of the dual problem, leads to the following error representation ,

$$\begin{aligned} \mathcal{M}(u) - \mathcal{M}(u_h) &= \mathcal{M}(u - u_h) \\ &= a^*(z, u - u_h) \\ &= a(u - u_h, z) \\ &= L(z) - a(u_h, z) \\ &= r(z) = r(z - z_h). \end{aligned}$$

So, the error is exactly represented by the residual of the dual solution,

$$\mathcal{M}(u) - \mathcal{M}(u_h) = r(z).$$

An adaptive algorithm seeks to determine a mesh size, $h = h(x)$, in a specific tolerance starting from an initial coarse mesh, and refine in those cells where the error indicator remains large.

For the Poisson equation, we take the goal functional to be defined as,

$$\mathcal{M}(u) = \int_\Omega u dx. \tag{36}$$

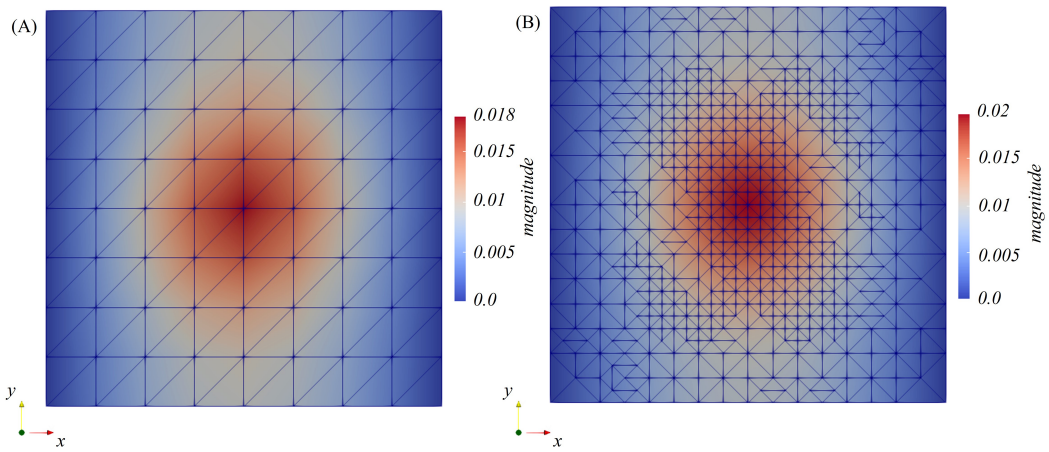

Fig. 6.: (A) Computational mesh and results for the Poisson equation, (B) Computational mesh and results for the Poisson equation after grid local refinement.

In Figure 6, we present the solution of Poisson equation with zero Dirichlet conditions. At the middle of the domain, we apply a two–dimensional Gaussian distribution, given by the expression described in equation (32). We observe that locally refining the computational grid with the AFEM described above, and introducing the goal functional of equation (36), the results in the domain of interest are capturing in detail the numerical solution of the Poisson equation. The given tolerance for the simulations is 10^{-5} and the final number of cells is increased to 1052 from the initial number of cells which was 128. This provide accurate results for the Poisson problem.

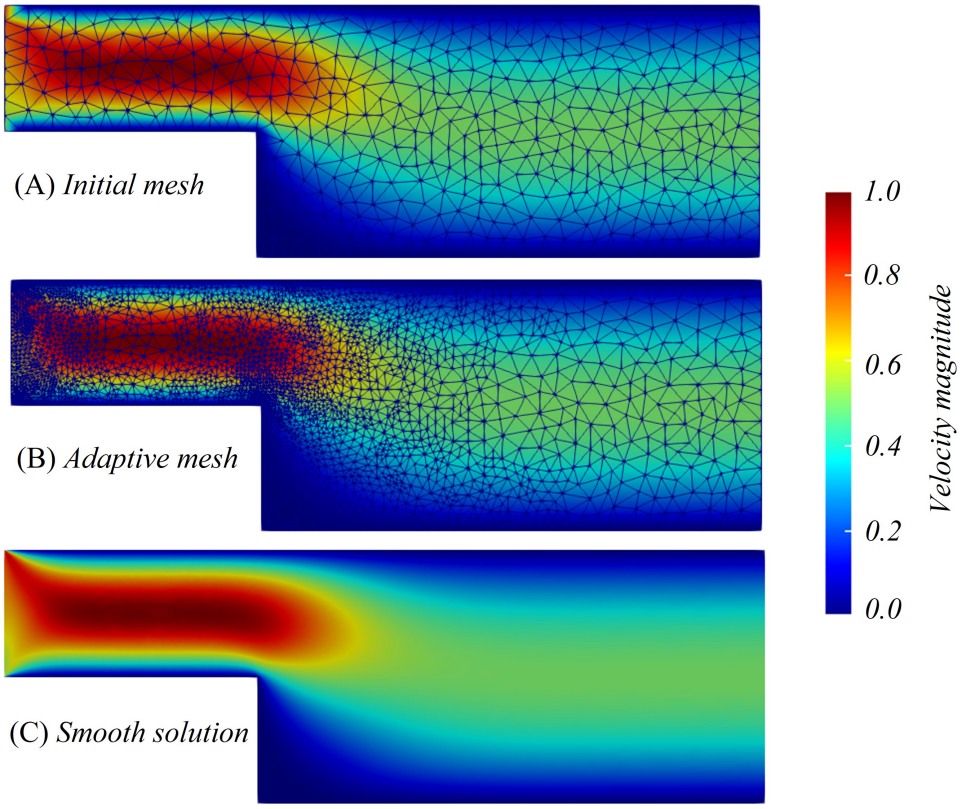

Fig. 7.: (A) The initial computational mesh for the backward facing step test problem, (B) The final computational mesh for the test problem. (C) The obtained smoothed results obtained from the AFEM.

Finally, we present similar results for the Stokes problem, where the mathematical formulation of the problem is discussed in a previous section. As depicted in Figure 7, we observe that locally refining the computational grid with the AFEM and introducing a similar goal functional of equation (36), the results in the back-

ward facing step test problem are substantially smoother, capturing in detail the numerical solution of the Stokes equation for the unknown vector field (velocity), $\bar{q}$ and pressure field, p. The given tolerance for the adaptive simulation is 10^{-7}. The final number of cells is increased to 7464 from the initial number, which was 890 triangular cells, providing accurate and smooth results for the test problem.

Conclusions: In this review chapter, the FEM is utilized for the numerical solution of ODEs and PDEs. We mainly focus on applying the method to fluid mechanics problems. Initially, we present the method along with the basic theorems and examples. We analyse the error estimates for linear problems and the base functions to distinguish the problem under consideration. We present the numerical solution of the Duffing equation and compare this solution with the analytical one. We further concentrate our attention on the two–dimensional Stokes and Navier–Stokes problems. We finally focus on presenting novel FEM variants such as the Discontinuous Galerkin (DG) method and adaptive methodologies (AFEM). These advanced methods provide reliable numerical results in all studied cases. This is achieved with the application of the FEM to "test problems", such as the backward facing step. We obtain all the numerical results utilizing the software programs MATLAB and FEniCS.

Acknowledgment: This research was partially supported by project "Dioni: Computing Infrastructure for Big-Data Processing and Analysis" (MIS No. 5047222) co–funded by European Union (ERDF) and Greece through Operational Program "Competitiveness, Entrepreneurship and Innovation", NSRF 2014-2020.

References

1. Antil, H., Hoppe, R.H., Linsenmann, C.: Path-following primal-dual interior-point methods for shape optimization of stationary flow problems. Journal of Numerical Mathematics **15**, 81–100 (2007)
2. Baker, G.A.: Finite element methods for elliptic equations using nonconforming elements. Mathematics of Computation **31**(137), 45–59 (1977)
3. Barkanov, E.: Introduction to the finite element method. Institute of Materials and Structures Faculty of Civil Engineering Riga Technical University pp. 1–70 (2001)
4. Bercovier, M., Pironneau, O.: Error estimates for finite element method solution of the stokes problem in the primitive variables. Numerische Mathematik **33**(2), 211–224 (1979)
5. Brenner, S., Scott, R.: The mathematical theory of finite element methods, vol. 15. Springer Science & Business Media (2007)
6. Chen, L., Asai, K., Nonomura, T., Xi, G., Liu, T.: A review of backward-facing step (bfs) flow mechanisms, heat transfer and control. Thermal Science and Engineering Progress **6**, 194–216 (2018)
7. Cockburn, B.: Discontinuous galerkin methods. ZAMM-Journal of Applied Mathe-

matics and Mechanics/Zeitschrift für Angewandte Mathematik und Mechanik: Applied Mathematics and Mechanics **83**(11), 731–754 (2003)
8. Cockburn, B., Karniadakis, G.E., Shu, C.W.: The development of discontinuous galerkin methods. In: Discontinuous Galerkin Methods, pp. 3–50. Springer (2000)
9. Cockburn, B., Karniadakis, G.E., Shu, C.W. (eds.): Discontinuous Galerkin Methods. Springer Berlin Heidelberg (2000). DOI 10.1007/978-3-642-59721-3. URL `https://doi.org/10.1007/978-3-642-59721-3`
10. Delfour, M., Hager, W., Trochu, F.: Discontinuous galerkin methods for ordinary differential equations. Mathematics of Computation **36**(154), 455–473 (1981)
11. Gander, M.J., Wanner, G.: From euler, ritz, and galerkin to modern computing. Siam Review **54**(4), 627–666 (2012)
12. Karakatsani, F., Makridakis, C.: A posteriori estimates for approximations of time-dependent stokes equations. IMA Journal of numerical analysis **27**(4), 741–764 (2006)
13. Lesaint, P., Raviart, P.A.: On a finite element method for solving the neutron transport equation. Publications mathématiques et informatique de Rennes (S4), 1–40 (1974)
14. Logg, A., Mardal, K.A., Wells, G.: Automated solution of differential equations by the finite element method: The FEniCS book, vol. 84. Springer Science & Business Media (2012)
15. Mbah, G.C., Ibeh, K.K.: Application of the finite element method to solving the duffing equation of ground motion. Global Journal of Pure and Applied Sciences **26**(1), 65–71 (2020)
16. Mu, L., Ye, X.: A simple finite element method for the stokes equations. Advances in Computational Mathematics **43**(6), 1305–1324 (2017)
17. Nochetto, R.H., Siebert, K.G., Veeser, A.: Theory of adaptive finite element methods: an introduction. In: Multiscale, nonlinear and adaptive approximation, pp. 409–542. Springer (2009)
18. Ølgaard, K.B., Logg, A., Wells, G.N.: Automated code generation for discontinuous galerkin methods. SIAM Journal on Scientific Computing **31**(2), 849–864 (2009)
19. Petropoulou, E.N., Xenos, M.A.: Qualitative, approximate and numerical approaches for the solution of nonlinear differential equations. In: Applications of Nonlinear Analysis, pp. 611–664. Springer (2018)
20. Raptis, A., Kyriakoudi, K., Xenos, M.A.: Finite element analysis in fluid mechanics. In: Mathematical Analysis and Applications, pp. 481–510. Springer (2019)
21. Reddy, J.: An introduction to the finite element method, vol. 1221. McGraw-Hill New York (2010)
22. Tezduyar, T.E., Mittal, S., Ray, S., Shih, R.: Incompressible flow computations with stabilized bilinear and linear equal-order-interpolation velocity-pressure elements. Computer Methods in Applied Mechanics and Engineering **95**(2), 221–242 (1992)
23. Thatcher, R.: Locally mass-conserving taylor–hood elements for two-and three-dimensional flow. International journal for numerical methods in fluids **11**(3), 341–353 (1990)
24. Xenos, M.A., Felias, A.C.: Nonlinear dynamics of the kdv-b equation and its biomedical applications. In: Nonlinear Analysis, Differential Equations, and Applications, pp. 765–793. Springer (2021)
25. Zhao, Y., Zhang, X., Ho, S.L., Fu, W.: An adaptive mesh method in transient finite element analysis of magnetic field using a novel error estimator. IEEE transactions on magnetics **48**(11), 4160–4163 (2012)
26. Zienkiewicz, O.C., Cheung, Y.K.: Finite Element Method in Structural & Continuum Mechanics. McGraw Hill (1967)

27. Zienkiewicz, O.C., Taylor, R.L., Zhu, J.Z.: The finite element method: its basis and fundamentals. Elsevier (2005)